

# Intrinsically disordered region of Talin's FERM domain functions as an initial PIP<sub>2</sub> recognition site

Jannik Buhr<sup>1,2</sup>, Florian Franz<sup>1,2</sup>, and Frauke Gräter<sup>1,2,\*</sup>

<sup>1</sup>Heidelberg Institute for Theoretical Studies

<sup>2</sup>Interdisciplinary Center for Scientific Computing, Heidelberg University

\*Correspondence: Frauke.Graeter@h-its.org

**ABSTRACT** Focal adhesions (FAs) mediate the interaction of the cytoskeleton with the extracellular matrix (ECM) in a highly dynamic fashion. Talin is a central regulator, adaptor protein and mechano-sensor of focal adhesion complexes. For recruitment and firm attachment at FAs, Talin's N-terminal FERM domain binds to phosphatidylinositol 4,5-bisphosphate (PIP<sub>2</sub>)-enriched membranes. A newly published autoinhibitory structure of Talin, where the known PIP<sub>2</sub> interaction sites are covered up, lead us to hypothesize that a hitherto less examined loop insertion of the FERM domain acts as an additional and initial site of contact. We evaluated direct interactions of Talin with a PIP<sub>2</sub> membrane by means of atomistic molecular dynamics (MD) simulations. We show that this unstructured, 33-residue-long loop strongly interacts with PIP<sub>2</sub> and can facilitate further membrane contacts, including the canonical PIP<sub>2</sub> interactions, by serving as a flexible membrane anchor. Under force as present at FAs, the extensible FERM loop ensures Talin to maintain membrane contacts when pulled away from the membrane by up to 7 nm. We identify key basic residues of the anchor mediating the highly dynamic Talin-membrane interaction. Our results put forward an intrinsically disordered loop as a key and highly adaptable PIP<sub>2</sub> recognition site of Talin and potentially other PIP<sub>2</sub>-binding mechano-proteins.

**SIGNIFICANCE** FERM domains are modular domains that often harbor PIP<sub>2</sub> binding sites and serve as anchoring points to membranes. Talin's FERM domain features a peculiar long and disordered loop, the function of which has remained fully elusive. We here show by means of atomistic Molecular Dynamics simulations that the loop serves as a first PIP<sub>2</sub> interaction site and flexible anchor to the membrane. This provides mechanistic insight into the role of intrinsically disordered regions in protein–membrane interactions.

## INTRODUCTION

### Tip

This is a draft and as such subject to change. The source repository for this manuscript lives at <https://github.com/hits-mbm-dev/paper-talin-loop>. The manuscript and poster are available in multiple formats:

- manuscript web/html: <https://hits-mbm-dev.github.io/paper-talin-loop/>
- manuscript print/pdf: <https://hits-mbm-dev.github.io/paper-talin-loop/index.pdf>
- poster web/html: <https://hits-mbm-dev.github.io/paper-talin-loop/poster.html>
- poster print/pdf: <https://hits-mbm-dev.github.io/paper-talin-loop/poster.pdf>

Cells critically sense the mechanics of their environment at cell adhesion sites for a multitude of biological processes. Contact with the extracellular matrix and surrounding cells regulates growth, differentiation, motility and even apoptosis (1–4). The multiprotein focal adhesion complex is responsible for translating between and integrating biochemical and mechanical signals for both outside-in and inside-out activation (5, 6).

At the center of the focal adhesion complex sits the adaptor protein Talin, which dynamically unfolds and refolds under force (7). A schematic of Talin can be seen in Figure 1a. Through interaction with integrin tails (dark green) (8), which in turn interact with collagen fibers via their heads, it links the extracellular matrix to the intracellular cytoskeleton by directly interacting with actin. Talin also features specific interactions with the membrane. Their formation, mechanical stability and role in mechanosensing remain to be fully resolved.

Talin contains an N-terminal FERM domain (F for 4.1 protein, E for ezrin, R for radixin and M for moesin), which is composed of the subdomains F0 to F3 and provides a link to the cytosolic side of the plasma membrane (9). It does so via a conserved binding motif for phosphatidylinositol 4,5-bisphosphate ( $\text{PIP}_2$ ), which is enriched at active focal adhesion sites (10–12). The main  $\text{PIP}_2$  binding sites are located in F2 and F3 (highlighted as red spheres in Figure 1a).

Notably, the Talin1 FERM domain differs from other FERM proteins through the addition of the F0 subdomain, which is connected to F1 via a charged interface, as well as an insertion in F1, a flexible loop with helical propensity and basic residues (13). Additionally, Talin's FERM domain exists in an extended conformation, as opposed to the cloverleaf-like conformation of other FERM proteins (14). F3 also has a binding site for  $\beta$ -integrin tails (15) and is partly responsible for the enrichment of  $\text{PIP}_2$  at the membrane through a binding site for PIPK $\gamma$  (16). A second integrin binding site is located in the rod domain 11 (R11) (17). Talin interacts with the cytoskeleton through actin binding sites (F2-F3, R4-R8, R13-DH) (18). The review by Klapholz et al. (19) provides an excellent overview of the many interaction sites of Talin and their central role in the focal adhesion complex.

The mechanistic role of the disordered F1 loop in the many aspects of Talin function remains elusive. Its overall positive charge renders it a prime candidate as a  $\text{PIP}_2$  binding site. However, previous studies only identified a minor role of the loop in  $\text{PIP}_2$  binding compared to F2-F3 (20, 21). On the other hand, the F1 loop has been shown to contribute to Talin-mediated integrin activation (13).

It was previously shown that F3 can interact with R9, which impedes integrin activation (22). Furthermore, in a recently determined cryo-electron microscopy structure of autoinhibited Talin1, Dedden et al. (23) showed that the rod domains R9 and R12 shield the established  $\text{PIP}_2$  binding surface and the integrin binding site in F3 (see Figure 1b, Figure 1c). This beckons the question how this autoinhibition can be resolved. Song et al. (12) previously investigated a fragment of Talin consisting of F2-F3 and an inhibiting rod segment and suggested a pull-push mechanism, whereby negatively charged  $\text{PIP}_2$  attracts its positively charged binding surface on F2-F3 and simultaneously repels the negatively charged surface of the inhibitory rod segment. However, this still leaves open the question of how Talin can establish a first contact with the membrane and remain within a sufficient proximity for this effect to kick in.

We hypothesized that the flexible F1 loop inserted into Talin's FERM domain serves as an additional  $\text{PIP}_2$  interaction site. As such it would be readily accessible

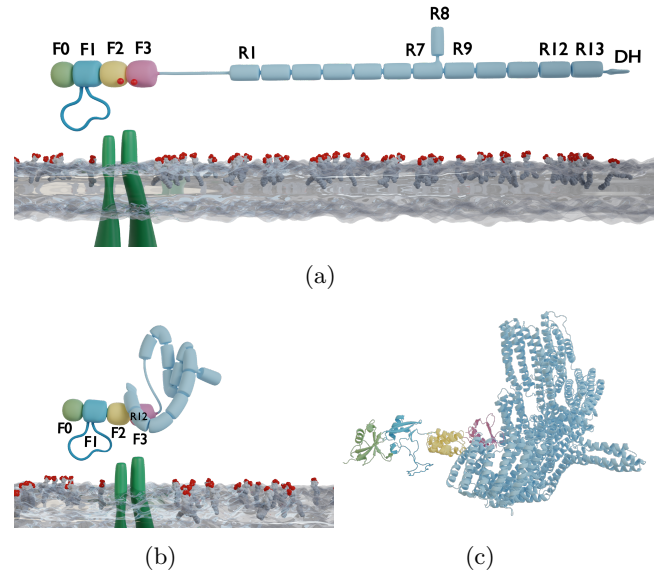


**Figure 1:** A schematic overview of Talin and our simulation setup. **a)** A schematic rendering of full-length Talin over a POPC membrane enriched with  $\text{PIP}_2$  in the upper leaflet. The subdomains under scrutiny in this publication, namely F0-F3, which comprise the N-terminal FERM domain (or Talin head), are highlighted in pastel colors (green, cyan, yellow, magenta). The two major  $\text{PIP}_2$  binding sites in F2-F3 are marked with red spheres. The Talin rod segments (or Talin tail) are numbered R1 to R13. Note that under physiological conditions, with Talin experiencing force from bound actin, the angle between the FERM domain and the Talin rod would be more akin to 30° as opposed to the linear structure shown here for illustrative purposes. Tails of an integrin  $\alpha$  and  $\beta$  heterodimer reaching through the lipid bilayer are represented in green. **b)** A schematic rendering of the autoinhibited structure of Talin as crystallized by Dedden et al. (23) in combination with a cartoon representation in **c)**. The completed FERM structure by Elliott et al. (14), with our addition of the modelled F1 loop, is fitted to the autoinhibited structure, as the latter does not include F0F1 due to their flexibility. The complete FERM structure can be explored interactively in the context of our simulation system in the Supplementary Materials. The main  $\text{PIP}_2$ -binding sites in F2-F3 are occluded by rod domain 12.

to PIP<sub>2</sub> even in Talin's autoinhibited conformation and would further mechanically stabilize Talin's interaction with the membrane. To test this hypothesis, we modelled the loop, which, due to its high flexibility, is not included in crystal structures of the FERM domain, such as PDB-ID 3IVF by Elliot et al. (14).

With a complete structure of the Talin FERM domain, we investigated the role of the F1 loop through atomistic molecular dynamics (MD) simulations, which had previously also proven useful to detect the recognition of PIP<sub>2</sub> in membranes by PH domains (24) or the FERM domain of Focal Adhesion Kinase (25).

In F0F1 simulations, we found the loop to have a clear propensity to interact with the PIP<sub>2</sub>-containing membrane. It is able to establish a first contact with the membrane even from unfavorable initial orientations due to its large search volume. Furthermore, we show with simulations of the full-length FERM domain that once the loop has established an initial contact, it can anchor the FERM domain to the membrane and establish the known major binding sites in F2-F3.

These results provide mechanistic insight Talin-PIP<sub>2</sub> interactions and highlight the role of secondary intrinsically disordered binding surfaces for membrane recognition.

## MATERIALS AND METHODS

### Molecular dynamics with GROMACS

MD simulations were performed with GROMACS (26, 27) version 2020.03 (28). A crystal structure of the Talin FERM domain by Elliot et al. (14) with the PDB-ID 3IVF was used as the basis of all simulations.

The deleted or missing residues (134-172) belonging to the F1 domain loop were modeled using MODELLER (29, 30) via the interface to Chimera (31), followed by equilibration with GROMACS. The resulting conformation was compared to an NMR structure of the F1 domain (PDB-ID 2KC2) by Goult et al. (13). The missing residue M1 was also added. Residues D125 and E126 are missing from our structure and the missing residues I399 and L400 were not modeled. This leaves us with a sequence from residue 1 to 398 with a shift by 2 in numbering compared to the canonical TLN1\_MOUSE Talin-1 sequence (uniprot ID P26039) after residue 124. Simulations were performed with the CHARMM36 force field. Topologies, including the membrane, were generated with the CHARMM-GUI web app (32-34) and GROMACS tools. All simulations used the TIP3P water model and were neutralized with 0.15 mol/L of NaCl. A 6-step equilibration was performed after gradient decent energy minimization while gradually relieving restraints on protein and membrane atoms. Production runs used a timestep of

2 fs, a Verlet cut-off scheme for Van-der-Waals interactions and the Particle Mesh Ewald (PME) method for long-range electrostatics. NPT-ensembles were achieved by Nosé-Hoover temperature coupling (35, 36) and Parrinello-Rahman pressure coupling (37). An example .mdp-file can be found in the Supplementary Materials.

The initial equilibrium simulation of the completed FERM domain was run for 75 ns. Subsequently, the root mean squared fluctuation (RMSF) was calculated with GROMACS tools.

The F0F1 FERM sub domains (residues 1 to 197) were simulated to evaluate protein-membrane association using a rotational sampling approach. This entailed placing the protein 1.5 nm away from a 1-palmitoyl-2-oleoyl-glycero-3-phosphocholine (POPC) membrane in a total of 60 orientations spanning a rotation of 360 degrees. The protein was rotated in such a way that the respective closest residue had the same distance to the membrane for the 0° and the 180° starting positions. 6 replicates of each orientation were run for 200 ns each. However, due to a hardware failure, 2 of these 360 runs are corrupted and thus excluded from the analysis. Of the 119 lipids in the upper leaflet of the POPC membrane, 12 lipids were replaced with PIP<sub>2</sub>, which results in a physiological concentration of 10% PIP<sub>2</sub>.

From this rotational sampling, we selected representative conformations with loop-membrane interactions as the basis of 6 equilibrium simulations of the complete FERM domain over a POPC membrane with 26 PIP<sub>2</sub> lipids out of a total of 273 lipids in the upper leaflet. Each simulation ran for 400 ns. The initial conformations for perpendicular pulling simulations of the F0F1 subdomains to gauge interaction strength were also chosen from the rotational sampling set.

Distance information was extracted from trajectories with gromacs tools interfaced via CONAN (38).

### Automation, Data Analysis and Availability

Setup scripts written in bash are available for all simulations shown in this work. Computations for data analysis were tracked with the targets R package (39). Plots were generated with ggplot2 (40). Interactive structure representations are embedded using Mol\* (41). Schematic visualizations were rendered with blender (42) and VMD (43). Files relevant to this work that are too big to be uploaded to this repository, such as trajectories and blender files, will be uploaded to a separate location. This manuscript was generated with quarto (44-46).

## RESULTS

### The F1 loop can act as a point of first contact

The high flexibility of the F1 loop gave us the confidence to model it from sequence. It retained its flexibility in equilibrium simulations (Figure 7a), which in combination with comparisons to NMR structures (13) confirmed this approach. The resulting system that provides the basis for our simulations can be explored interactively in the Supplementary Materials.

When simulating only F0F1 over a POPC membrane containing 10% PIP<sub>2</sub>, we noticed that the F1 loop had a clear propensity to establish contact with the membrane. Once the contact had been established, the protein was anchored strongly enough for more contacts to evolve with time, pulling the protein onto the membrane (Figure 2a). In order to control for a potential bias towards the loop as a result of the starting position, we performed a rotational sampling of the system, where the starting angle of the loop with respect to the membrane was varied across 60 equally spaced angles. Figure 2b shows that independent of the starting position, the loop is able to find the membrane and bind to it, though this does happen earlier in the simulation when the loop starts favorably oriented towards the membrane (Figure 3a). However, even in its most unfavorable starting orientation (180°, oriented away from the membrane) the loop is able to find the membrane due to the large search space it can cover with its high flexibility (see Figure 7a).

Once a contact has been made, it becomes exceedingly unlikely for F0F1 to dissociate from the membrane (Figure 3b). Out of 358 runs<sup>1</sup>, 89 runs never made contact with the membrane, but out of the 269 that did, only 10 eventually dissociated. Thus, the simulated timeframe of 200 ns per trajectory allowed for the observation of some reversibility of FERM–PIP<sub>2</sub> binding, albeit only for weakly bound cases and at a small rate of 3.7%. Dissociation from the membrane never occurred on the simulated time scale after more than 3 residues had already made contact.

Figure 4 highlights the residues involved in the interaction of F0F1 with PIP<sub>2</sub>. We observe a number of prominent lysines and arginines, both positively charged residues, across the whole F0F1 fragment to compensate for the negative charge on PIP<sub>2</sub>. The loop region, highlighted with a grey backdrop in Figure 4a, is particularly dense in positively charged residues, albeit the number of PIP<sub>2</sub> contacts per basic residue is only marginally higher in this region than elsewhere. Arginines and lysines in regions outside

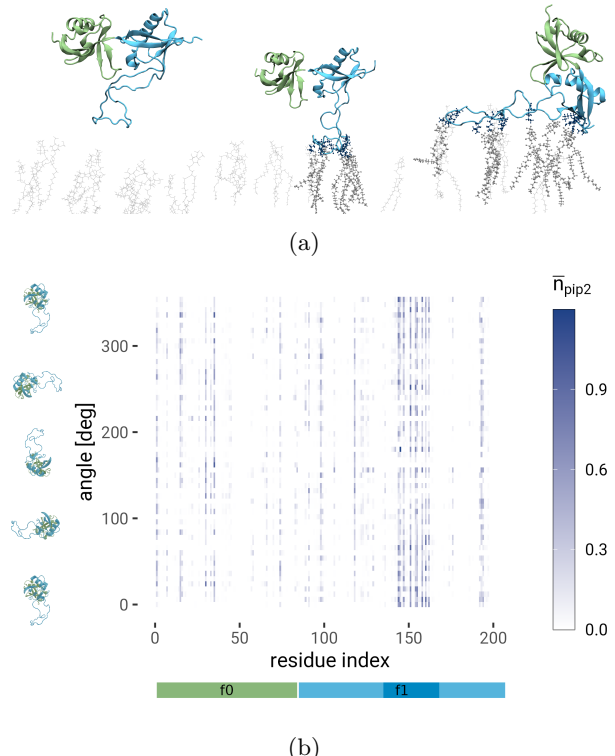


Figure 2: Rotational sampling of F0F1 reveals the lipid binding capabilities of the F1 loop. **a)** Snapshots from a simulation involving F0F1 over a POPC membrane containing 10% PIP<sub>2</sub> in the upper leaflet. POPC is not rendered and PIP<sub>2</sub> is shown as light grey stick models that turn thicker for those molecules that are currently interacting with residues of the protein. Those residues in question are then shown as dark blue stick models. **b)** Time-averaged number of PIP<sub>2</sub> molecules bound per residue along the F0F1 sequence (x-axis) as a heatmap summarizing 358 simulations from a rotational sampling, with the starting angle on the y-axis. We sampled 60 different starting positions, rotated equally spaced around the horizontal axis, with 6 replicates each. Each simulation is 200 ns long. 0° corresponds to the loop pointing downwards towards the membrane, as shown in the smaller renders to the left of the heatmap.

<sup>1</sup>6 replicas each for 60 angles minus 2 runs lost to a storage failure

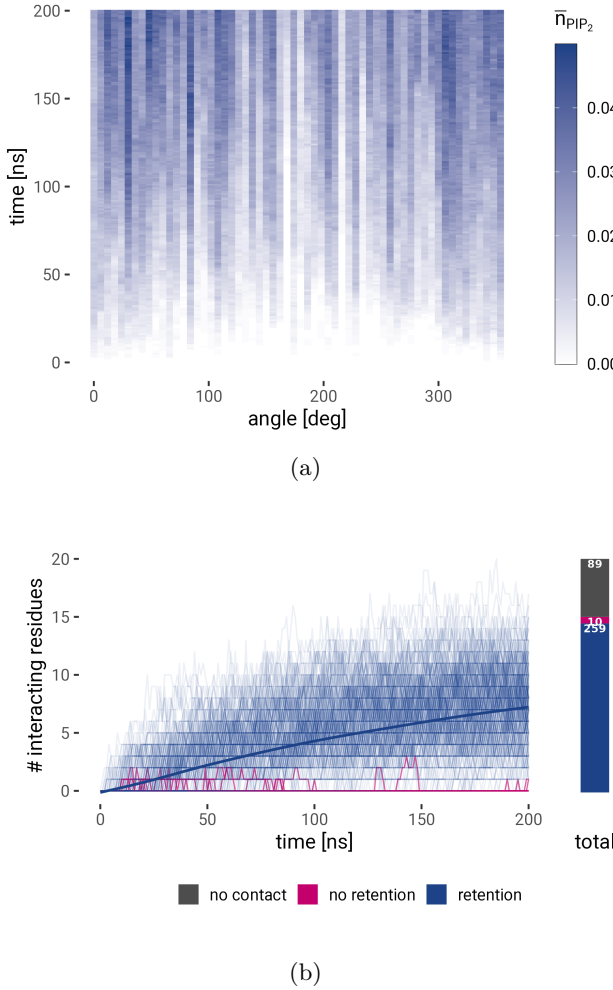


Figure 3: Loop-PIP<sub>2</sub> contacts dynamically accumulate and are mediated by basic residues. **a)** Heatmap of the time evolution of the average number of PIP<sub>2</sub> molecules per residue at the respective time (y-axis) and angle (x-axis). **b)** Time evolution (x-axis) of the number of residues currently interacting with PIP<sub>2</sub> (y-axis) shows binding and unbinding events and an eventual accumulation of contacts. Unbinding becomes exceedingly unlikely as the number of contacts increases.

of the disordered loop complement the binding once initial contacts have been established with the loop, and further strengthen the interaction. F0 at the N-terminus (left) is quite flexible as well (see Figure 7a) and can thus reasonably contribute towards membrane binding. The C-terminus of the F1 domain, instead, harbors the interface towards the F2 domain and the two PIP<sub>2</sub>-interacting residues identified here will be more occluded *in vivo*. Indeed, simulations of the full-length FERM domain in the later part of this work do not show these interactions anymore (Figure 6a).

### The F1 loop maintains and further facilitates formation of FERM-PIP<sub>2</sub> interactions

To examine the strength of the PIP~2 interactions and the role of the F1 loop in maintaining it, we pulled F0F1 vertically off the membrane in additional force-probe MD simulations (Figure 5). An exemplary render of one of the simulations can be seen in Figure 5a. Pulling F0F1 off the membrane requires peak forces of 100–120 pN, during which the interacting residues only very gradually loose contact (Figure 5), as the high flexibility of F1-loop allows the residues to remain in contact even as the distance increases up to a delta of 7 nm. Replicate 4 stands out as the highest curve, as in this run the interactions were so strong that a total of 3 molecules of PIP<sub>2</sub> were pulled out of the membrane (1 by F0 and 2 by the F1 loop). A snapshot of this can be seen in Figure 7e. This highlights the strong anchoring capabilities of the F1 loop.

As seen in Figure 5c, during pulling residues not belonging to the F1 loop loose contact first, while the loop stays attached. The F1 loop works in conjunction with the F0 subdomain (see Figure 7d). Their high flexibility allows them to remain in contact with the membrane over large distances, which would allow for a spring-like re-establishing of more contacts should the force be alleviated. In two cases the last interacting residue was part of the F1 loop, while in three cases the N-terminus of the F0 domain stayed attached for longest.

Having established the prominent role of the F1-loop in positioning F0F1 at the membrane and establishing PIP<sub>2</sub> contacts, we next examined this role in the larger context of the full FERM domain. 6 independent simulations were initiated with the full-length FERM domain oriented in such that the tip of the F1-loop was in contact with at least one molecule of PIP<sub>2</sub> with varying local environments (see Section for one example). These simulations highlight the prominent role of the F1-loop in membrane interactions, now in the context of the full-length FERM domain (Figure 6a, compare to Figure 4a). They also reproduce the canonical PIP<sub>2</sub> contacts in F2 and F3 known from previous studies, val-

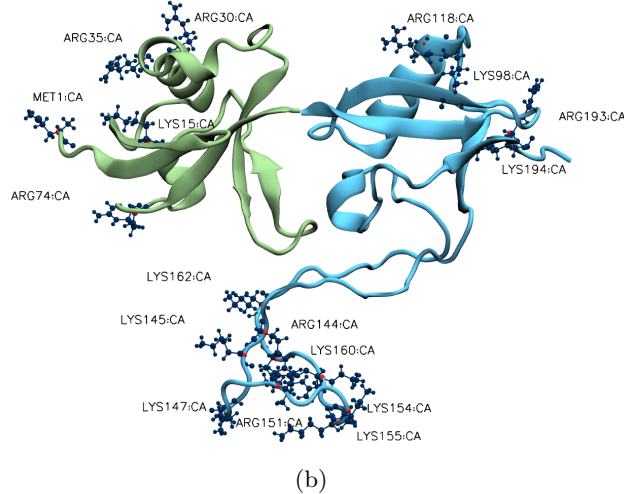
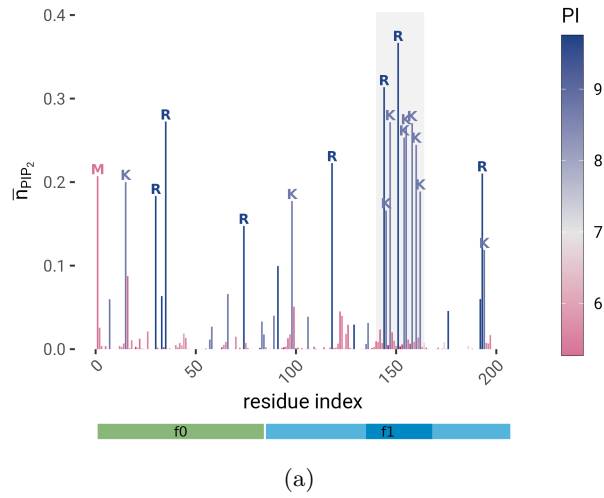


Figure 4: Lysine and arginine residues are crucial for the  $\text{PIP}_2$ -interaction of F0F1. **a)** The average number of  $\text{PIP}_2$  molecules ( $\bar{n}_{\text{PIP}_2}$ ) interacting (see Figure 7b for the interaction distance definition) with the individual residues per frame across all simulations of the rotational sampling that made contact with the membrane. Color represents the isoelectric point of the amino acid in isolation (blue = basic, magenta = acidic). A number of very prominent lysines can be observed, as well as a cluster of residues belonging to the F1 loop, which is highlighted with a grey backdrop. The most prominent residues are highlighted in **b)**. For the print version it is a snapshot render. The video is also available here: <https://youtu.be/s5yya0XeNTA>.

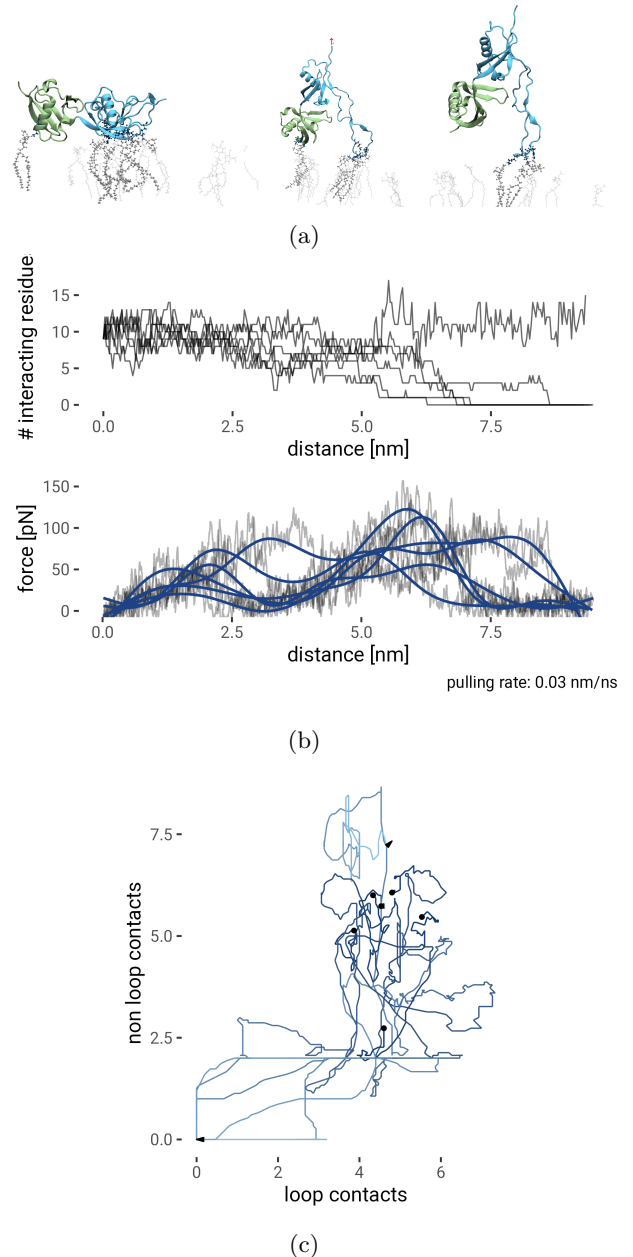


Figure 5: Vertical pulling of F0F1 highlights the F1 loop's flexibility and ability to maintain contacts with the membrane over large distances. **a)** Representative render of one of 6 force-probe MD simulations pulling F0F1 off the membrane. For the print version we show a series of three snapshots, the video is available here: <https://youtu.be/-eZ2orx7QRE>. It starts from a snapshot of F0F1 in its bound conformation taken from the rotational sampling and gets pulled upwards from its C-terminus. **b)** Number of interacting residues (top panel) and the force (bottom panel) as a function of distance (x-axis) as F0F1 gets pulled off the membrane at a constant rate of 0.03 nm/ns. **c)** Time evolution of the number of contacts for residues belonging to the F1 loop (x-axis) and other residues (y-axis). Lighter shades of blue correspond to a later time in the simulation. Black dots mark the starting positions. The non-loop contacts are mostly supplied by the residues of the F0 N-terminus also shown in Figure 4a.

idating our MD simulations. The highlighted residues include K272 of F2 and K316, K324, E342, and K343 of F3, which have been shown to be crucial for the membrane interaction of Talin and subsequent integrin activation by Chinthalapudi et al. (20). Importantly, the loop shows a very dense cluster of PIP<sub>2</sub> interactions, with interaction scores ( $\bar{n}_{PIP_2}$ ) very similar to these previously known PIP<sub>2</sub>-interacting residues. The F1 loop thus complements these known binding sites with an additional specific binding site, again comprising primarily lysines.

## DISCUSSION AND OUTLOOK

Using atomistic MD simulations, we provide mechanistic insight into the membrane recognition dynamics of Talin. Our simulations propose a new mode of interaction that helps to explain how Talin can bind the membrane even when its main PIP<sub>2</sub> (and integrin) binding sites in F2 and F3 (20) (see figure Figure 6b ) are blocked by autoinhibition (23). Specifically, we find the unique unstructured, 33-residue-long insertion into the F1 domain, the F1 loop, to provide a strong interaction anchor to PIP<sub>2</sub>-containing membranes.

Overall, the FERM-membrane interaction mode is not characterized by singular binding sites interacting with one molecule of PIP<sub>2</sub> each, as would be the conclusion from crystallographic data alone. Rather the cumulative diffuse interaction of multiple PIP<sub>2</sub> with multiple residues is what keeps the protein anchored to the membrane. This is particularly evident in the interaction with the flexible F1 loop, but also in the F0 domain. While crystal structures of proteins in complex with PIP<sub>2</sub> typically show a one-to-one ratio of lipid per binding site (20, 47, 48), possibly due to the nature of the experimental method, our simulations suggest multiple PIP<sub>2</sub> molecules binding simultaneously. Similar results have been observed for Pleckstrin Homology (PH) domain proteins by Naughton et al. (49). According to their study, this simultaneous binding of multiple PIP<sub>2</sub> molecules contributes to the high affinity of the membrane interaction.

Our MD simulations suggest that the F1 loop can find favorable interactions with PIP<sub>2</sub> across large distances and in a large search volume. We find this to be the disordered loop's high flexibility. The F1 loop can maintain the membrane contacts when Talin is pulled off of the membrane over distances as large as 7 nm. A similar mechanism has also been shown by Shoemaker et al. (50) and was fittingly coined "fly-casting". In the aforementioned publication they focus on the interaction of unfolded regions with DNA. Our simulations now provide an example for the concept applied to protein-lipid interactions. It is well worth noting that, although we mention the greater search space of the F1 loop as its advantage in recognizing PIP<sub>2</sub>, it has also been argued that the kinetic advantage of the fly-casting mechanism comes mainly from the reduction in free energy as the disordered region folds around the interaction target (51). This can also be argued here, as the loop can flexibly adapt its conformation to the membrane and the dynamic distribution of PIP<sub>2</sub> lipids therein. As such it can bind in a multivalent fashion, with several basic residues binding to several PIP<sub>2</sub> lipids.

Fast binding kinetics are crucial for Talin's function at focal adhesion sites. As the PIP<sub>2</sub> concentrations increases at the active focal adhesion site, Talin's FERM

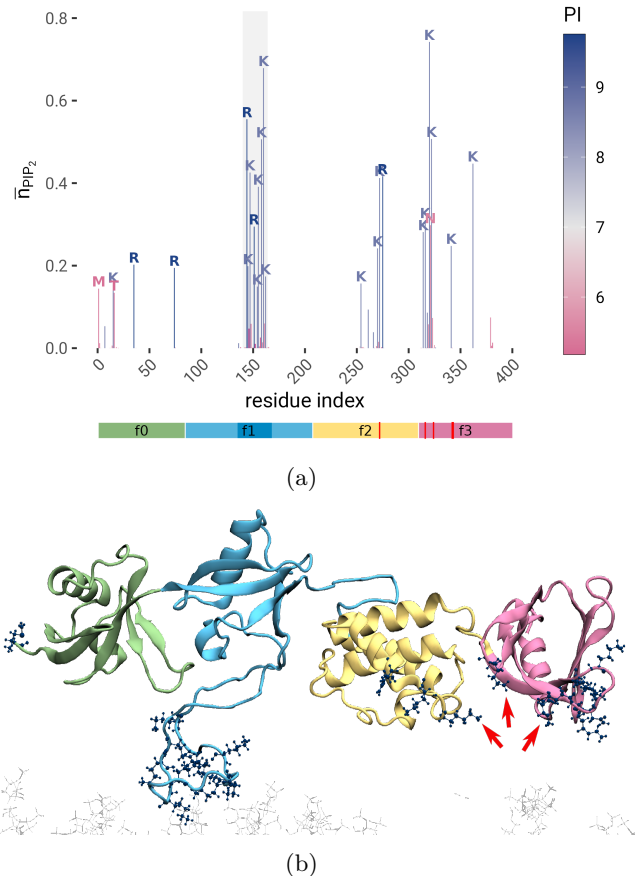


Figure 6: Simulation of the full-length FERM domain over a 10% PIP<sub>2</sub>-membrane. **a)** The average number of PIP<sub>2</sub> molecules interacting with the individual residues across 6 simulations. Color represents the isoelectric point of the amino acid in isolation (blue = basic, magenta = acidic). The known PIP<sub>2</sub> interaction sites K272 of F2 and K316, K324, E342, and K343 of F3 (20) are highlighted with red lines on the x-axis colorbar and can also be seen in the cartoon representation in **b)** where the interacting residues with a score greater than 0.2 are displayed as dark blue stick models.

F1 loop can perform rapid recognition. The flexibility of the loop also allows it to anchor the protein at the membrane even when being stretched under force (up to a delta of 7 nm, as seen in Figure 5). This is akin to the elastic response seen in focal adhesion kinase (FAK) under force, in which a 49-residue-long linker allows for buffering of the force (52). Here, Talin's F1 loop can extend and thereby maintain the interactions, which could help rapid rebinding when the force is relieved.

In our force probe simulations, we pulled F0F1 orthogonally off the membrane. This allowed us to assess the full extension and force resistance of the loop. *In vivo*, however, Talin's FERM domain is subjected to forces acting at a 30° angle. This might imply an additional function for the FERM domain. As it is dragged along the membrane, the diffuse interactions of the F1 loop and main interaction sites in F2-F3 with PIP<sub>2</sub> would increase lateral friction along the membrane as the PIP<sub>2</sub> concentration increases. This could further localize Talin at active focal adhesion sites even in the presence of forces acting parallel to the membrane.

We conclusively show that the F1 loop is able to interact with the membrane even from most unfavorable orientations. We propose that Talin mutants lacking the loop, or specifically the basic residues in said loop, will show reduced or at least slowed-down focal adhesion maturation, increased lateral diffusion of Talin under force, and faster focal adhesion disassembly.

Recognition is only the first step. The mechanistic details of how Talin's autoinhibition is resolved remain to be shown by larger simulations including the inhibiting rod segment. These larger-scale simulations might then be able to provide evidence for the push-pull mechanism proposed by Song et al. (12) or might reveal how the early F1-loop mediated membrane interactions identified in this study might effect the subsequent steps for Talin activation. In conclusion, we propose positively charged, intrinsically disordered regions in Talin's FERM domain and potentially other PIP<sub>2</sub>-binding domains to promote recognition and to help maintain the membrane interaction under force.

## AUTHOR CONTRIBUTIONS

Conceived and designed the experiments: JB FF FG. Performed the experiments: JB FF. Analyzed the data: JB FF. Contributed reagents/materials/analysis tools: FF. Wrote the paper: JB FF.

## ACKNOWLEDGMENTS

This work was supported by the Klaus Tschira Foundation and the European Research Council (ERC) under the European Union's Horizon 2020 research and innovation programme (grant agreement No. 101002812).

## REFERENCES

- Vogel, V., and M. Sheetz. 2006. Local force and geometry sensing regulate cell functions. *Nature Reviews Molecular Cell Biology*. 7:265–275.
- Oakes, P.W., and M.L. Gardel. 2014. Stressing the limits of focal adhesion mechanosensitivity. *Current Opinion in Cell Biology*. 30:68–73.
- Schiller, H.B., and R. Fässler. 2013. Mechanosensitivity and compositional dynamics of cell-matrix adhesions. *EMBO reports*. 14:509–519.
- Miroshnikova, Y.A., H.Q. Le, D. Schneider, T. Thalheim, M. Rübsam, N. Bremicker, J. Polleux, N. Kamprad, M. Tarantola, I. Wang, M. Balland, C.M. Niessen, J. Galle, and S.A. Wickström. 2018. Adhesion forces and cortical tension couple cell proliferation and differentiation to drive epidermal stratification. *Nature Cell Biology*. 20:69–80.
- Thamilselvan, V., and M.D. Basson. 2004. Pressure activates colon cancer cell adhesion by inside-out focal adhesion complex and actin cytoskeletal signaling. *Gastroenterology*. 126:8–18.
- Pelletier, A.J., T. Kunicki, Z.M. Ruggeri, and V. Quaranta. 1995. The Activation State of the Integrin αIIbβ3 Affects Outside-in Signals Leading to Cell Spreading and Focal Adhesion Kinase Phosphorylation \*. *Journal of Biological Chemistry*. 270:18133–18140.
- Yao, M., B.T. Goult, B. Klapholz, X. Hu, C.P. Toseland, Y. Guo, P. Cong, M.P. Sheetz, and J. Yan. 2016. The mechanical response of talin. *Nature Communications*. 7:11966.
- Tadokoro, S., S.J. Shattil, K. Eto, V. Tai, R.C. Liddington, J.M. de Pereda, M.H. Ginsberg, and D.A. Calderwood. 2003. Talin Binding to Integrin β Tails: A Final Common Step in Integrin Activation. *Science*. 302:103–106.
- Chishti, A.H., A.C. Kim, S.M. Marfatia, M. Lutchman, M. Hanspal, H. Jindal, S.-C. Liu, P.S. Low, G.A. Rouleau, N. Mohandas, J.A. Chassis, J.G. Conboy, P. Gascard, Y. Takakuwa, S.-C. Huang, E.J.B. Jr, A. Bretscher, R.G. Fehon, J.F. Gusella, V. Ramesh, F. Solomon, V.T. Marchesi, S. Tsukita, S. Tsukita, M. Arpin, D. Louvard, N.K. Tonks, J.M. Anderson, A.S. Fanning, P.J. Bryant, D.F. Woods, and K.B. Hoover. 1998. The FERM domain: A unique module involved in the linkage of cytoplasmic proteins to the membrane. *Trends in Biochemical Sciences*. 23:281–282.

10. Mani, T., R.F. Hennigan, L.A. Foster, D.G. Conrady, A.B. Herr, and W. Ip. 2011. **FERM Domain Phosphoinositide Binding Targets Merlin to the Membrane and Is Essential for Its Growth-Suppressive Function.** *Molecular and Cellular Biology.* 31:1983–1996.
11. Das, T., K. Safferling, S. Rausch, N. Grabe, H. Boehm, and J.P. Spatz. 2015. **A molecular mechanotransduction pathway regulates collective migration of epithelial cells.** *Nature Cell Biology.* 17:276–287.
12. Song, X., J. Yang, J. Hirbawi, S. Ye, H.D. Perera, E. Goksoy, P. Dwivedi, E.F. Plow, R. Zhang, and J. Qin. 2012. **A novel membrane-dependent on/off switch mechanism of talin FERM domain at sites of cell adhesion.** *Cell Research.* 22:1533–1545.
13. Goult, B.T., M. Bouaouina, P.R. Elliott, N. Bate, B. Patel, A.R. Gingras, J.G. Grossmann, G.C.K. Roberts, D.A. Calderwood, D.R. Critchley, and I.L. Barsukov. 2010. **Structure of a double ubiquitin-like domain in the talin head: A role in integrin activation.** *The EMBO Journal.* 29:1069–1080.
14. Elliott, P.R., B.T. Goult, P.M. Kopp, N. Bate, J.G. Grossmann, G.C.K. Roberts, D.R. Critchley, and I.L. Barsukov. 2010. **The Structure of the Talin Head Reveals a Novel Extended Conformation of the FERM Domain.** *Structure(London, England:1993).* 18:1289–1299.
15. Calderwood, D.A., R. Zent, R. Grant, D.J.G. Rees, R.O. Hynes, and M.H. Ginsberg. 1999. **The Talin Head Domain Binds to Integrin  $\beta$  Subunit Cytoplasmic Tails and Regulates Integrin Activation \*.** *Journal of Biological Chemistry.* 274:28071–28074.
16. Calderwood, D.A., I.D. Campbell, and D.R. Critchley. 2013. **Talins and kindlins: Partners in integrin-mediated adhesion.** *Nature Reviews Molecular Cell Biology.* 14:503–517.
17. Horwitz, A., K. Duggan, C. Buck, M.C. Beckerle, and K. Burridge. 1986. **Interaction of plasma membrane fibronectin receptor with talin—a transmembrane linkage.** *Nature.* 320:531–533.
18. McCann, R.O., and S.W. Craig. 1997. **The I/LWEQ module: A conserved sequence that signifies F-actin binding in functionally diverse proteins from yeast to mammals.** *Proceedings of the National Academy of Sciences.* 94:5679–5684.
19. Klapholz, B., and N.H. Brown. 2017. **Talin – the master of integrin adhesions.** *Journal of Cell Science.* 130:2435–2446.
20. Chinthalapudi, K., E.S. Rangarajan, and T. Izard. 2018. **The interaction of talin with the cell membrane is essential for integrin activation and focal adhesion formation.** *Proceedings of the National Academy of Sciences of the United States of America.* 115:10339–10344.
21. Saltel, F., E. Mortier, V.P. Hytönen, M.-C. Jacquier, P. Zimmermann, V. Vogel, W. Liu, and B. Wehrle-Haller. 2009. **New PI(4,5)P<sub>2</sub>- and membrane proximal integrin-binding motifs in the talin head control B3-integrin clustering.** *Journal of Cell Biology.* 187:715–731.
22. Banno, A., B.T. Goult, H. Lee, N. Bate, D.R. Critchley, and M.H. Ginsberg. 2012. **Subcellular Localization of Talin Is Regulated by Inter-domain Interactions \*.** *Journal of Biological Chemistry.* 287:13799–13812.
23. Dedden, D., S. Schumacher, C.F. Kelley, M. Zacharias, C. Biertümpfel, R. Fässler, and N. Mizuno. 2019. **The Architecture of Talin1 Reveals an Autoinhibition Mechanism.** *Cell.* 179:120–131.e13.
24. Buyan, A., A.C. Kalli, and M.S.P. Sansom. 2016. **Multiscale Simulations Suggest a Mechanism for the Association of the Dok7 PH Domain with PIP-Containing Membranes.** *PLOS Computational Biology.* 12:e1005028.
25. Zhou, J., C. Aponte-Santamaría, S. Sturm, J.T. Bullerjahn, A. Bronowska, and F. Gräter. 2015. **Mechanism of Focal Adhesion Kinase Mechanosensing.** *PLOS Computational Biology.* 11:e1004593.
26. Berendsen, H.J.C., D. van der Spoel, and R. van Drunen. 1995. **GROMACS: A message-passing parallel molecular dynamics implementation.** *Computer Physics Communications.* 91:43–56.
27. Abraham, M.J., T. Murtola, R. Schulz, S. Páll, J.C. Smith, B. Hess, and E. Lindahl. 2015. **GROMACS: High performance molecular simulations through multi-level parallelism from laptops to supercomputers.** *SoftwareX.* 1–2:19–25.
28. Lindahl, Abraham, Hess, and van der Spoel. 2020-01-01, 2020-01. **GROMACS 2020 source code.** Zenodo.
29. Martí-Renom, M.A., A.C. Stuart, A. Fiser, R. Sánchez, F. Melo, and A. Sali. 2000. **Comparative protein structure modeling of genes and genomes.** *Annual Review of Biophysics and Biomolecular Structure.* 29:291–325.

30. Webb, B., and A. Sali. 2016. **Comparative Protein Structure Modeling Using MODELLER.** *Current Protocols in Protein Science.* 86:2.9.1–2.9.37.
31. Pettersen, E.F., T.D. Goddard, C.C. Huang, G.S. Couch, D.M. Greenblatt, E.C. Meng, and T.E. Ferrin. 2004. **UCSF Chimera—a visualization system for exploratory research and analysis.** *Journal of Computational Chemistry.* 25:1605–1612.
32. Brooks, B.R., C.L. Brooks, A.D. Mackerell, L. Nilsson, R.J. Petrella, B. Roux, Y. Won, G. Archontis, C. Bartels, S. Boresch, A. Caflisch, L. Caves, Q. Cui, A.R. Dinner, M. Feig, S. Fischer, J. Gao, M. Hodoscek, W. Im, K. Kuczera, T. Lazaridis, J. Ma, V. Ovchinnikov, E. Paci, R.W. Pastor, C.B. Post, J.Z. Pu, M. Schaefer, B. Tidor, R.M. Venable, H.L. Woodcock, X. Wu, W. Yang, D.M. York, and M. Karplus. 2009. **CHARMM: The biomolecular simulation program.** *Journal of Computational Chemistry.* 30:1545–1614.
33. Jo, S., T. Kim, V.G. Iyer, and W. Im. 2008. **CHARMM-GUI: A web-based graphical user interface for CHARMM.** *Journal of Computational Chemistry.* 29:1859–1865.
34. Lee, J., X. Cheng, J.M. Swails, M.S. Yeom, P.K. Eastman, J.A. Lemkul, S. Wei, J. Buckner, J.C. Jeong, Y. Qi, S. Jo, V.S. Pande, D.A. Case, C.L. Brooks, A.D. MacKerell, J.B. Klauda, and W. Im. 2016. **CHARMM-GUI Input Generator for NAMD, GROMACS, AMBER, OpenMM, and CHARMM/OpenMM Simulations Using the CHARMM36 Additive Force Field.** *Journal of Chemical Theory and Computation.* 12:405–413.
35. Hoover, W.G. 1985. **Canonical dynamics: Equilibrium phase-space distributions.** *Physical Review A.* 31:1695–1697.
36. Nosé, S. 1984. **A unified formulation of the constant temperature molecular dynamics methods.** *The Journal of Chemical Physics.* 81:511–519.
37. Parrinello, M., and A. Rahman. 1981. **Polymorphic transitions in single crystals: A new molecular dynamics method.** *Journal of Applied Physics.* 52:7182–7190.
38. Mercadante, D., F. Gräter, and C. Daday. 2018. **CONAN: A Tool to Decode Dynamical Information from Molecular Interaction Maps.** *Biophysical Journal.* 114:1267–1273.
39. Landau, W.M. 2021. The targets R package: A dynamic Make-like function-oriented pipeline toolkit for reproducibility and high-performance computing. *Journal of Open Source Software.* 6:2959.
40. Wickham, H. 2016. **Ggplot2: Elegant graphics for data analysis.** Springer-Verlag New York.
41. Sehnal, D., S. Bittrich, M. Deshpande, R. Svobodová, K. Berka, V. Bazgier, S. Velankar, S.K. Burley, J. Koča, and A.S. Rose. 2021. **Mol\* Viewer: Modern web app for 3D visualization and analysis of large biomolecular structures.** *Nucleic Acids Research.* 49:W431–W437.
42. Community, B.O. 2018. **Blender - a 3D modelling and rendering package.**
43. Humphrey, W., A. Dalke, and K. Schulten. 1996. **VMD – Visual Molecular Dynamics.** *Journal of Molecular Graphics.* 14:33–38.
44. Allaire, J.J., C. Teague, C. Scheidegger, Y. Xie, and C. Dervieux. 2022. **Quarto.**
45. Xie, Y. 2015. **Dynamic documents with R and knitr.** Second. Boca Raton, Florida: Chapman and Hall/CRC.
46. Aden-Buie, G. 2022. **Betterposter: A better scientific poster.**
47. Chinthalapudi, K., V. Mandati, J. Zheng, A.J. Sharff, G. Bricogne, P.R. Griffin, J. Kissil, and T. Izard. 2018. **Lipid binding promotes the open conformation and tumor-suppressive activity of neurofibromin 2.** *Nature Communications.* 9:1338.
48. Jian, X., W.-K. Tang, P. Zhai, N.S. Roy, R. Luo, J.M. Gruschus, M.E. Yohe, P.-W. Chen, Y. Li, R.A. Byrd, D. Xia, and P.A. Randazzo. 2015. **Molecular Basis for Cooperative Binding of Anionic Phospholipids to the PH Domain of the Arf GAP ASAP1.** *Structure.* 23:1977–1988.
49. Naughton, F.B., A.C. Kalli, and M.S.P. Sansom. 2018. **Modes of Interaction of Pleckstrin Homology Domains with Membranes: Toward a Computational Biochemistry of Membrane Recognition.** *Journal of Molecular Biology.* 430:372–388.
50. Shoemaker, B.A., J.J. Portman, and P.G. Wolynes. 2000. **Speeding molecular recognition by using the folding funnel: The fly-casting mechanism.** *Proceedings of the National Academy of Sciences of the United States of America.* 97:8868–8873.
51. Huang, Y., and Z. Liu. 2009. **Kinetic Advantage of Intrinsically Disordered Proteins in Coupled Folding–Binding Process: A Critical Assessment of the “Fly-Casting” Mechanism.** *Journal of Molecular Biology.* 393:1143–1159.

## SUPPLEMENTARY MATERIAL

### Simulation System

**i** Note

This interactive display is only available in the web version: <https://hits-mbm-dev.github.io/paper-talin-loop/>

### Scripts

Data analysis code is available at [https://hits-mbm-dev.github.io/paper-talin-loop/\\_analysis.html](https://hits-mbm-dev.github.io/paper-talin-loop/_analysis.html) and in the repository at <https://github.com/hits-mbm-dev/paper-talin-loop>. Raw trajectories are available here: TODO (upload in process)

### Supplementary Plots and Tables

#### Molecular Dynamics Parameters

```

integrator          = md
dt                 = 0.002
nsteps             = 100000000
cutoff-scheme      = Verlet
nstlist            = 20
rlist              = 1.2
coulombtype       = pme
rcoulomb           = 1.2
vdwtype            = Cut-off
vdw-modifier       = Force-switch
rvdw_switch        = 1.0
rvdw               = 1.2
tcoupl             = Nose-Hoover
tc_grps            = SYSTEM
tau_t              = 1.0
ref_t              = 303.15
pcoupl             = Parrinello-Rahman
pcoupltype         = semiisotropic
tau_p              = 5.0
compressibility    = 4.5e-5 4.5e-5
ref_p              = 1.0 1.0
constraints         = h-bonds
constraint_algorithm = LINCS
continuation        = yes
nstcomm            = 100
comm_mode          = linear
comm_grps          = SYSTEM
refcoord_scaling   = com

```

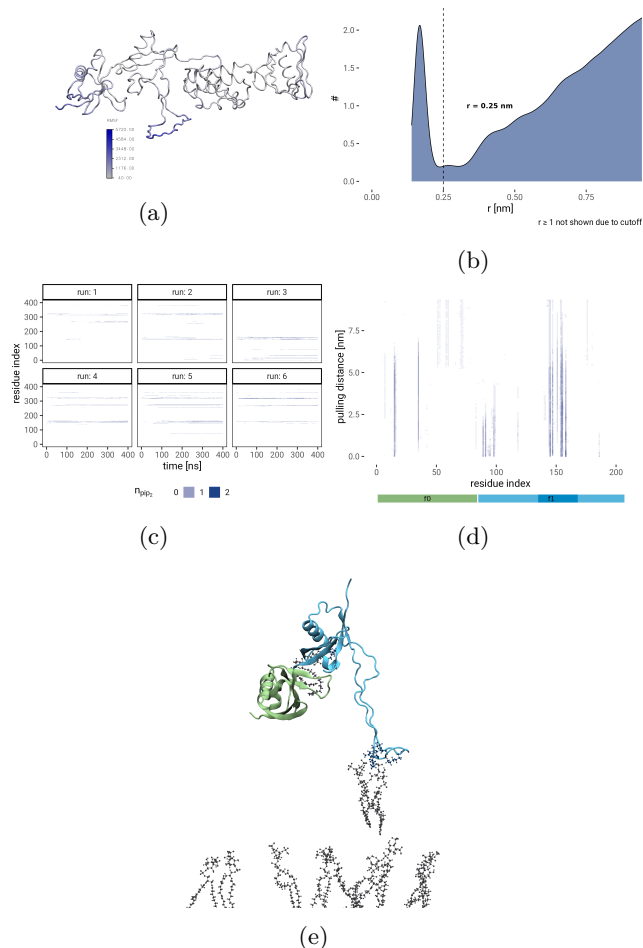


Figure 7: **a)** RMSF [nm] of the  $\text{c}\alpha$  of individual residues in an equilibrium simulation shown by coloring the backbone. The loop is highly flexible. **b)** A density plot of distances between PIP<sub>2</sub> and the protein residues to decide on a cutoff for defining interactions. A distance of 0.25 nm was chosen. **d)** A closer look at the residues involved in the interaction during pulling reveals the instrumental role of both the F1 loop as well as the F0 subdomain in keeping the connection to the membrane. **e)** Run 4 of the vertical pulling of F0F1. Interactions between the protein and PIP<sub>2</sub> were so strong that a total of 3 molecules of PIP<sub>2</sub> (gray) were pulled out of the membrane (1 by F0 (green) and 2 by the F1 loop (blue)).

Table 1: Top residues interacting with F0F1

residue	mean_n_pip
M 1	0.118
K 15	0.114
R 30	0.104
R 35	0.155
K 98	0.101
R 118	0.127
R 144	0.179
K 147	0.155
R 151	0.209
K 154	0.144
K 155	0.152
K 158	0.154
K 160	0.139
K 162	0.107
R 193	0.120

Table 2: Top residues interacting with FERM

residue	mean_n_pip
M 1	0.144
K 15	0.154
T 16	0.134
R 35	0.202
R 74	0.195
R 144	0.555
K 145	0.199
K 147	0.426
R 151	0.295
K 154	0.149
K 155	0.391
K 158	0.506
K 160	0.679
K 162	0.174
K 254	0.157
K 270	0.242
K 272	0.412
R 275	0.416
K 314	0.281
K 316	0.310
K 320	0.742
N 321	0.298
K 322	0.507
K 341	0.248
K 362	0.447